Supplementary Information:

Highly Compressed Two-Dimensional Form of Water at Ambient Conditions

Sarp Kaya, Daniel Schlesinger, Susumu Yamamoto, John T. Newberg, Hendrik Bluhm, Hirohito Ogasawara, Tom Kendelewicz**,** Gordon E. Brown Jr.**,** Lars G. M. Pettersson and Anders Nilsson

Contents:

1. Experimental details

1.1 Methods and sample preparation

BaF_2(111) crystals (Surface Preparation Lab) were cleaved in vacuum and dry nitrogen environment. Before cleavage, the crystals were mounted on the sample holder and thermal contact with the Peltier element, which is used to reduce the sample temperature, was maintained by using a carbon tape. Temperature was measured by K-type thermocouples placed on a Peltier element in AP-XPS setup and spot-welded on the sample holder in the UHV chamber. Due to differential charging in dry conditions, XPS could not be used to quantify the carbon contamination level of the freshly cleaved samples. Instead, XAS measurements at the C K-edge were performed and signatures of adventitious carbon, C=C, CO, C-H and CH_xO_y were not detected. The amount of carbon accumulated on the surface in wet conditions can be determined by XPS and is presented in Fig. S1. By taking relative ionization cross-sections into account, the

adventitious carbon was estimated to be less than 5 % of a monolayer.

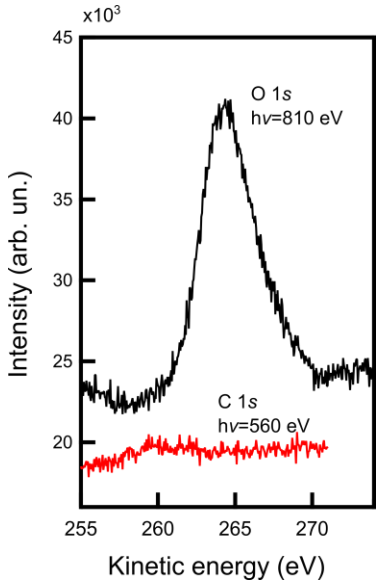

Figure S1. O 1*s* and C 1*s* XPS spectra indicate the low level of adventitious carbon. Data was acquired at 30 % RH, in 1.5 Torr water.

Water was dosed on LN_2 cooled samples via a directional pulse valve in a UHV chamber. The base pressure of the chamber was better than 5×10^{-10} Torr. Water was outgassed by freeze-pump-thaw cycles several times before use. BaF_2(111) crystals were cleaved in a dry N_2 atmosphere. LDA was formed by depositing water on BaF_2(111) at 100 K. Annealing to induce structural changes in LDA was performed by radiative heating. Coverage is approximated by the amount of water dosed onto the surface, which is cross-correlated by following O 1*s* XPS spectra of a water monolayer formed on Ni(111) in exactly the same way. At 100 K, the sticking probability of water was assumed to be 1. The O 1*s* binding energy difference between monolayer and multilayer ice was used to determine monolayer completion on Ni(111). Coverage of the annealed ice films was estimated by integrating the intensity of the O K-edge XAS spectra in the near-edge region. O K-edge XAS spectra of LDA and crystalline ice were recorded through total electron yield (TEY), using a XAS detector equipped with retarding field grids and a microchannel plate (MCP). Spectra were normalized to incoming photon flux and the background from the bare BaF_2(111) substrate was subtracted.

Milli-Q water was introduced into the AP-XPS chamber via a variable leak valve and relative humidity (RH) was increased by reducing the sample temperature using the Peltier

element. Prior to use, water was outgassed by repeated freeze-pump-thaw cycles.

1.2 Determination of the coverage of the ambient water films

The evolution of water films on $BaF_2(111)$ with increasing relative humidity (RH) is monitored by recording O 1*s* XPS spectra at 1.5 Torr water (Fig S2(a)). In measurements on ambient water, gas phase molecules contribute to XPS spectra together with the surface features being investigated. As a free molecule, the binding energy of the O 1*s* core level electrons is several eV higher than that of adsorbed water [1]. Besides, the cross section between the incoming synchrotron light and gas phase molecules within the frame of photoemitted electron trajectories determines the intensity of the gas phase peaks in the spectra. Fig S2(b) shows that the gas phase peak appearing at 528.4 eV partially overlaps with additional features on the high binding-energy side. The component at 532.0 eV corresponding to molecularly adsorbed water overlaps with a small shoulder at 529.5 eV, which is assigned to surface OH groups. The binding energies of adsorbed water and OH groups appear at several eV higher than nominal values due to charging issues. We note here that the energy scale is referenced to the F 1*s* binding energy. More importantly, the energy difference between these two peaks is 2.45 eV, which is similar to previous observations [2]. Fig S2(a) shows that the progressive increase of the O 1*s* intensity with increasing RH due to water adsorption is not accompanied by an increase in intensity from surface OH groups. At 95 % RH, the fraction of surface OH groups is negligible, much less than 10 % of a water monolayer, with very similar fraction at 7 % RH; thus they cannot account for the structural motifs of ambient water films.

Spectral broadening caused by surface charging at the initial stage of water adsorption (RH<15 %) is partially eliminated by the increase of water coverage as a function of RH. Differential charging due to accumulation of positive charge is a general phenomenon in conventional photoelectron spectroscopy of large band-gap [3] insulating materials like $BaF_2(111)$ and leads to shifts in the kinetic energy of the emitted electrons. However, at elevated pressures, Auger and secondary electrons emitted from gas phase molecules as well as from the adsorbates compensate the charging to a large extent [4]. Condensed water can be considered as a material with smaller band gap [5] in comparison to $BaF_2(111)$ which creates another channel to more effectively screen the differential charging in the substrate. We can therefore have two effects on the spectral line-shape dependence on water thickness; *i.e.* changes in the hypothetical water

structure or successive disappearance of charging. It is likely that water does not completely wet the overall surface up to 30-40 % RH [5] and therefore spectral broadening is observed. As can be seen from Fig S2(c) Ba 4*d* spectra suffer from charging-induced broadening up to 90 % RH, but no major changes in peak position are observed in 1.5 Torr. Moreover, Ba 4*d* spectra did not show any indication of BaO or $Ba(OH)_2$ formation. Dissolution of Ba^{2+} and F^- ions into water films is negligible because the solubility of BaF_2 is low (0.17 g/100 ml water 300 K) and no changes in apparent binding energies of the O 1*s* and Ba 4*d* spectra are observed.

The coverage of the adsorbed water films in ambient conditions was estimated by scaling the integrated O 1*s* XPS peak intensities of water films on $BaF_2(111)$ and the well-defined (5.4×10^{14} O atoms/cm^2) *p*(2×1)-O phase on Cu(110) in 1.5 Torr water ambient [6]. This ensures that under the same measurement conditions intensities of the surface species are comparable because the degree of scattering of emitted photoelectrons from adsorbed molecules by the gas phase molecules is the same. O 1*s* intensities from the *p*(2×1)-O phase on Cu(110) were normalized to the Cu 3*p* intensities and kinetic energies of the electrons were kept the same as kinetic energies measured from water films on $BaF_2(111)$ (KE=270 eV).

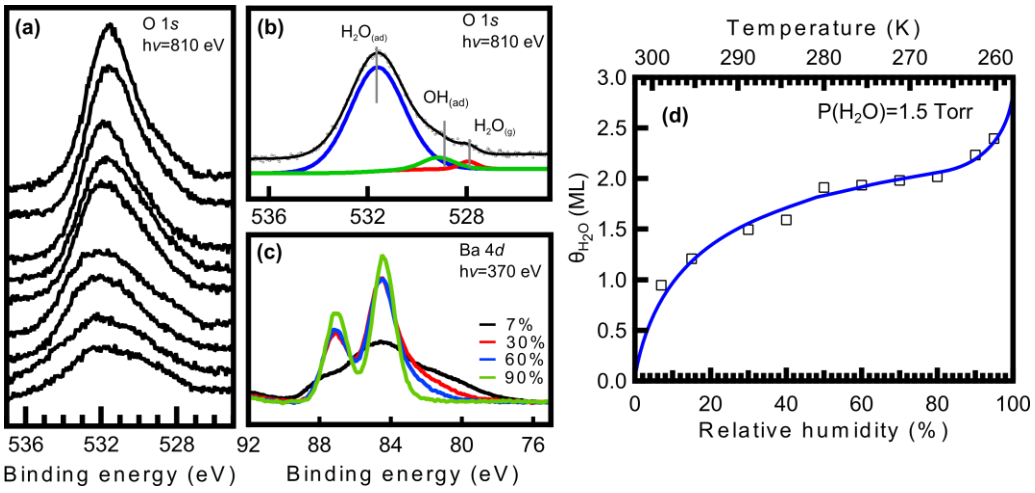

Figure S2. **(a)** O 1*s* XPS spectra of water on $BaF_2(111)$ in 1.5 Torr measured by raising RH from 7 % to 95 %. **(b)** O 1*s* XPS spectra of water at 90 % RH. **(c)** Ba 4*d* XPS spectra recorded at 7 %, 30 %, 60 %, and 90 % RH. Spectra were acquired in grazing incidence geometry, similar to XAS measurements and the energy scales were referenced to the binding energy of F 1*s* (684.3 eV^2) **(d)** Water uptake curve acquired by analysis of O 1*s* XPS spectra. The blue line is a guide to the eye.

The uptake curve shown in Fig S2(d), plotted in order to calibrate water coverage for XAS measurements, is in good agreement with the ones measured using IR spectroscopy [7]. Up to ~20 % RH, water coverage (as deduced from the O 1*s* intensity, Fig S2(a)) increases in an exponential fashion and then rises more gradually from ~20 % RH to 80 %. Above 80 % RH, water coverage increases in a fashion similar to what has been characterized as type II adsorption isotherms where multilayer growth sets in after completion of the first wetting layer. This type of uptake differs from Langmuir (Type I) behavior where uptake levels off after saturation coverage is reached. In line with this observation, a recent scanning force microscopy study [8] has shown that on BaF_2(111), water layers at 50 % RH tend to wet the major fraction of the surface, ruling out the possibility of 3D particle formation.

1.3 O K-edge XAS of thin-film water

O K-edge XAS spectra in 1.5 Torr water ambient were recorded by using the Auger electron yield technique (AEY) and an electron spectrometer (Phobios 150, Specs). In order to avoid contributions from gas phase XPS peaks, the kinetic energy window was set to detect electrons between 370 and 400 eV kinetic energy. Because the photon flux is modulated due to absorption by gas phase water molecules (middle spectrum in Fig. S3), photon flux measurements should be performed at the sample position. This obstacle was circumvented by using a highly ordered pyrolytic graphite (HOPG) sample which is inert to water adsorption. Within the energy scan range used for absorption measurements, C 1*s* spectra were recorded. Because XPS peak intensities are proportional to the incoming photon flux, any change due to absorption by gas phase water is reflected in the C 1*s* peak areas, and the outcome of this modulation can be seen in the bottom spectrum in Fig. S3. After XAS spectral normalization, a background from the BaF_2(111) surface (in 5 % RH, normalized to photon flux) was subtracted from each spectrum recorded at 30 %, 60 % and 90 % RH. To minimize x-ray induced structural changes, each spectrum was taken at a new spot.

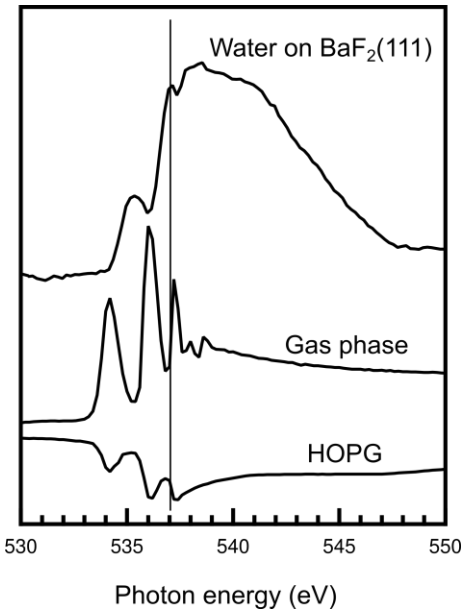

Figure S3. **(top)** Raw O K-edge XAS spectra of water on BaF_2(111) in 1.5 Torr water vapor, **(middle)** XAS spectra of gas phase water molecules, and **(bottom)** integrated areas of C 1*s* XPS peaks from HOPG in 1.5 Torr water vapor.

2. Simulation details

2.1 Dependence of the O-O pair correlation function on the water model

The differences in the Lennard-Jones and Coulomb terms in pair-potentials are the basic differences between the transferrable intermolecular potential (TIP3P, TIP4P, TIP4P/2005) and extended simple point charge (SPC/E) models that have been heavily used to model the properties of water in various conditions [9]. All three other models yielded an O-O pair-correlation between first layer water molecules similar to the results from the TIP4P/2005 model. As shown in Fig. S4, the second and the third coordination shells collapse to 3.3 and 6 Å and the number of molecules within the first coordination shell becomes smaller for all cases. The shell structure is less pronounced for TIP3P and SPC/E as also found in simulations of bulk water. Nevertheless, all models predict high density structures of the first-layer water on BaF_2(111) surfaces through inward collapse of the second shell.

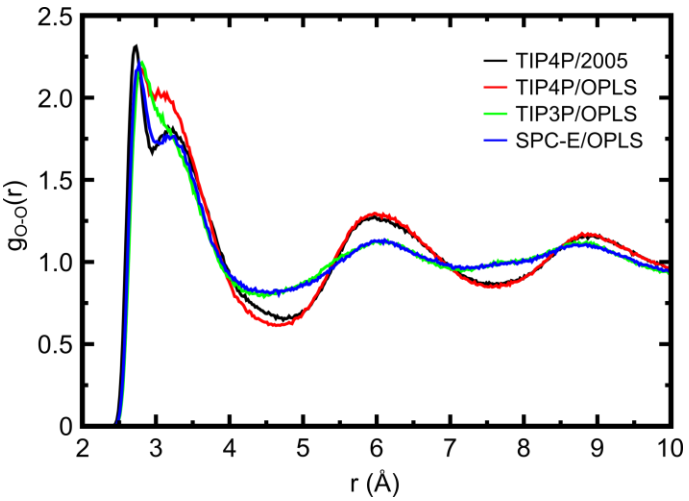

Figure S4. Comparison of the O-O pair-correlation functions in the first layer of H_2O on BaF_2(111) obtained with different water models. The crystal was described with the OPLS force field in all cases.

2.2 Dependence of the O-O pair-correlation function on the effective ionic charges

Coulomb interaction between partial charges within the water molecule and the ionic charges of the surface ions provides the dominant interaction in the system under consideration. Thus, the effective charges of the surface ions were expected to play a prominent role for the structure observed. MD simulations were performed with three different charge pairs for ions in the BaF_2(111) slab to investigate the influence on the O-O pair-correlation function (PCF) of water on the surface. The results are shown in Fig. S5. There is a clear effect of the changes in charge on the PCF. However, comparison to the bulk water O-O PCF calculated with the same method clearly shows that even an unrealistically weak charge pair (-0.5e, +1.0e) still results in a HDL-like PCF.

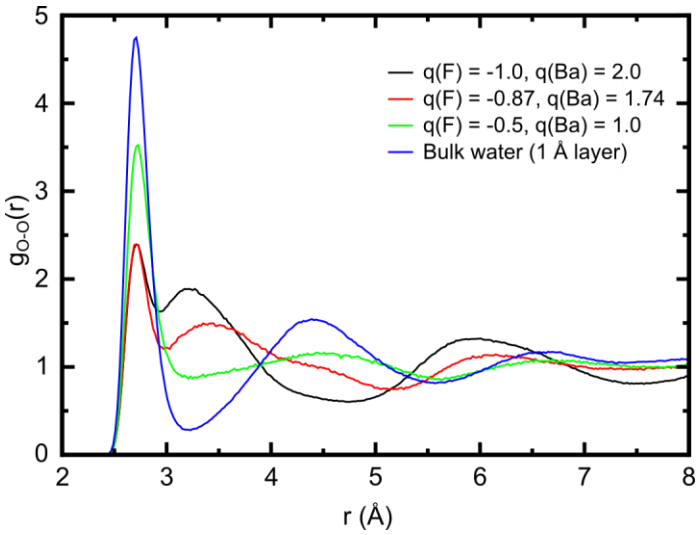

Figure S5. Comparison of first-layer O-O pair-correlation functions for water on BaF_2(111) with different effective ionic charges, as indicated. A bulk water O-O pair-correlation function obtained from a 1 Å thick slab through the simulation box (*i.e.* the same conditions and normalization as for the surface layer) is plotted for comparison.

2.3 Normalization of the pair-correlation function in the layer: definition

Pair-correlation functions were calculated in layers oriented parallel to the surface in order to investigate the structure of water close to the BaF_2(111) surface. These layers were given the thickness h = 1 Å. In order to account for the non-sphericity of the problem, a modified normalization is used.

The usual definition of a pair correlation function is

$$g(r[i]) = \frac{n\ i}{v\ i}\frac{V}{N}$$

where $n[i]$ is the number of oxygen pairs with distances binned in the interval ($r_{i+1}=r_i+dr$; r_i) called $r\ i$ with a maximal distance R, $v[i]$ is the associated volume difference between successive bins, V denotes the total volume, and N the total number of included molecules [10]. In order to modify the normalization appropriately, the above definition is used and the quantities on the right hand side are redefined according to the thin-slab geometry of the first and subsequent layers on the surface. Calculating the constant factor, the total volume is taken to be a spherical segment with the center of the sphere approximated to be in the central plane of the layer, and thus

$$\frac{V}{N} = \pi\, h \frac{R^2 + \frac{h^2}{6}}{N}.$$

The number of oxygen pairs n[i] per distance bin i=dist/dr is counted for all oxygen pairs present within the layer. Depending on the distance z of the central oxygen atom from the lower layer-limiting plane, three cases are distinguished (cf. Fig. S6):

1. The spherical shell is entirely inside the layer for very short distances (usual spherical norm).

   $(r_{i+1} < z) \quad (r_{i+1} < h - z)$:

   $$v\ i\ = \frac{4\pi}{3}(r_{i+1}^3 - r_i^3)$$

2. The spherical shell intersects with one of the two layer-limiting, parallel planes. The spherical cap outside the layer is thus to be subtracted from the full spherical shell.

   $(r_{i+1} > z) \quad (r_{i+1} < h - z)$:

   $$v\ i\ = \frac{4\pi}{3}\ r_{i+1}^3 - r_i^3\ -$$
   $$-[\frac{\pi}{3}\ r_{i+1} - z\ ^2\ \ 3\, r_{i+1} -\ r_{i+1} - z\ \ -\frac{\pi}{3}\ r_i - z\ ^2\ (3\, r_i - (r_i - z))]$$

   and analogously for $(r_{i+1} < z) \quad (r_{i+1} > h - z)$.

3. The spherical shell intersects both layer-limiting planes. This case is approximated by a cylinder volume, so that the pair-correlation function, with the definition of the constant N/V, converges to unity for large radii.

   $(r_{i+1} > z) \quad (r_{i+1} > h - z)$:

   $$v\ i\ = \pi\, h\, (r_{i+1}^2 - r_i^2)$$

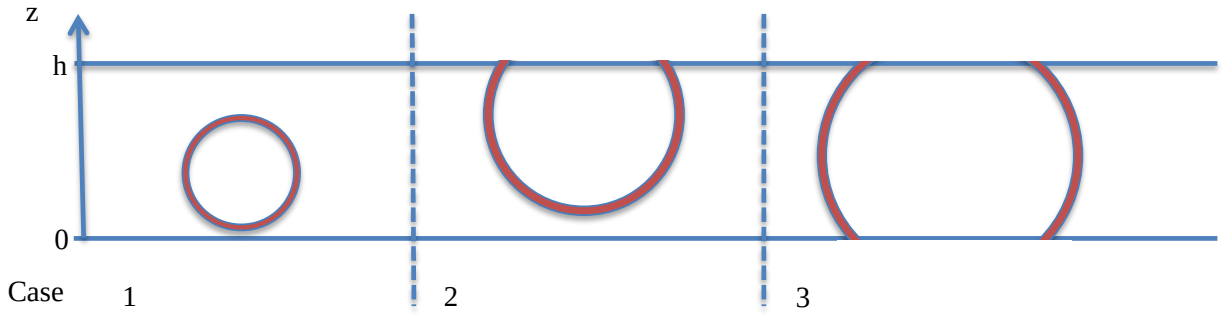

Figure S6. 2-dimensional sketch of the three cases distinguished in the layer-definition of the PCF thin-slab normalization described in the text.

For simplicity, the value for z was not measured for every central oxygen but chosen as $z = \frac{h}{4}$ in order to represent the asymmetrical situation in the second case above.

2.4 Energy calibration against Density Functional Theory

Adsorption energies of an isolated water molecule on a (3×3) four-layered BaF_2(111) slab have been calculated from energy-minimized simulation boxes using empirical force fields and from density functional theory (DFT) using different functionals for comparison and shown in Table S1 and Table S2. The real-space-grid based GPAW [11,12] code was used with a grid-spacing of 0.2 Å.

Table S1. Adsorption energies obtained with MD force-fields for two different surface ion charge pairs (energy minimized, same structure as for DFT calculation)

Water model (BaF_2 described by OPLS for all cases)	*Adsorption energy [kJ/mol], charge pair (-1.0e, +2.0e)*	*Adsorption energies [kJ/mol], charge pair (-0.87e, +1.74e)*
TIP4P/2005 (OPLS)	-41.2	-34.6
TIP4P (OPLS)	-37.1	-30.7
SPC/E (OPLS)	-33.5	-26.9
TIP3P (OPLS)	-27.0	-21.5

Table S2. Adsorption energies obtained from DFT:

Functional	Adsorption energy [kJ/mol]
BEEF-vdW [13]	-33.1
PBE [14]	-30.7
RPBE [15]	-14.0

It is clear that the different force-fields give values for the adsorption energies in good comparison to those obtained with DFT, in particular for the PBE and BEEF functionals, where the latter includes also non-local correlation describing van der Waals interactions. In quantum chemical calculations of ionic systems one typically finds lower charges than the nominal ones; in fact, using the intermediate charge pair brings the force-field values into even better agreement with the DFT values. Note, however, that the conclusions on a highly compressed contact layer are independent of force-field and charge-pair.

3. References

1. Bluhm, H. Photoelectron spectroscopy of surfaces under humid conditions. *J. Electron. Spectrosc.* **177**, 71 (2010).
2. Wu, Y. T., Mayer, J. T., Garfunkel, E. & Madey, T. E. X-ray photoelectron spectroscopy study of water-adsorption on BaF_2(111) and CaF_2(111) surfaces. *Langmuir* **10**, 1482 (1994).
3. Khenata, R. *et al.* Structural, electronic and optical properties of fluorite-type compounds. *Eur. Phys. J. B* **47**, 63 (2005).
4. Verdaguer, A., Segura, J. J., Fraxedas, J., Bluhm, H. & Salmeron, M. Correlation between charge state of insulating NaCl surfaces and ionic mobility induced by water adsorption: a combined ambient pressure x-ray photoelectron spectroscopy and scanning force microscopy study. *J. Phys. Chem. C* **112**, 16898 (2008).
5. Verdaguer, A. *et al.* Growth and structure of water on SiO_2 films on Si investigated by Kelvin probe microscopy and in situ x-ray spectroscopies. *Langmuir* **23**, 9699 (2007).
6. Andersson, K. *et al.* Autocatalytic water dissociation on Cu(110) at near ambient conditions. *J. Am. Chem. Soc.* **130**, 2793 (2008).
7. Sadtchenko, V., Conrad, P. & Ewing, G. E. H_2O adsorption on BaF_2(111) at ambient temperatures. *J. Chem. Phys.* **116**, 4293 (2002).
8. Verdaguer, A., Cardellach, M. & Fraxedas, J. Thin water films grown at ambient conditions on BaF_2(111) studied by scanning polarization force microscopy. *J. Chem. Phys.* **129**, 174705 (2008).
9. Mark, P. & Nilsson, L. Structure and dynamics of the TIP3P, SPC, and SPC/E water models at 298 K. *J. Phys. Chem. A* **105**, 9954 (2001).
10. Allen, M. P. & Tildesley, D. J. *Computer simulation of liquids*. (Oxford University Press: Oxford, 1987).
11. Mortensen, J. J., Hansen, L. B. & Jacobsen, K. W. Real-space grid implementation of the projector augmented wave method. *Phys. Rev. B* **71**, 035109 (2005).
12. Enkovaara, J. *et al.* Electronic structure calculations with GPAW: a real-space implementation of the projector augmented-wave method. *J. Phys.: Cond. Matter.* **22**, (2010).
13. Wellendorff, J. *et al.* Density functionals for surface science: Exchange-correlation model development with Bayesian error estimation. *Phys. Rev. B* **85**, 235149 (2012).
14. Perdew, J. P., Burke, K. & Ernzerhof, M. Generalized Gradient Approximation Made Simple. *Phys. Rev. Lett.* **77**, 3865 (1996).
15. Hammer, B., Hansen, L. B. & Nørskov, J. K. Improved adsorption energetics within density-functional theory using revised Perdew-Burke-Ernzerhof functionals. *Phys. Rev. B* **59**, 7413 (1999).